Scattering of Oceanic Internal Gravity Waves off Random Bottom Topography*

PETER MÜLLER AND NAIHUAI XU

Department of Oceanography, School of Ocean and Earth Science and Technology, University of Hawaii, Honolulu, Hawaii

(Manuscript received 1 April 1991, in final form 25 July 1991)

ABSTRACT

The scattering of oceanic internal gravity waves off random bottom topography is analyzed under the assumptions that (i) the height of the topography is smaller than the vertical wavelength and (ii) the slope of the topography is smaller than the wave slope. For each frequency, scattering redistributes the incoming energy flux in horizontal wavenumber space. The scattered wave field approaches an equilibrium state where the energy flux is equipartitioned in horizontal wavenumber space. For incoming red spectra, this implies a transfer from low to high wavenumbers. For typical internal wave and bottom spectra, about 6.8% of the incoming energy flux is redistributed. While this might be less than the flux redistribution caused by reflection off a critical slope, the scattering process transfers the energy flux to higher wavenumbers than the reflection process. Scattering might thus be equally or more efficient than reflection in causing high shears and mixing near the bottom.

1. Introduction

The interaction of internal gravity waves with bottom topography has been advocated as a process that results in mixing near the bottom. The interaction distorts the incoming waves in such a way that they are more likely to break and cause mixing. Such internal wave–induced bottom or boundary mixing might significantly contribute to basinwide mixing and explain the discrepancy between the diapycnal diffusivity observed in the ocean interior and the one required by basinwide heat and mass balances. Observations and theoretical arguments affirm boundary mixing caused by internal waves reflected off a critical slope. In this paper we show that internal waves scattered off short topographic irregularities might cause even more efficient mixing.

When the wavelength of the incident internal wave is much smaller than the radius of curvature of the topography, the wave is reflected as if encountering an infinite straight slope. The reflection laws then require that the magnitude of the wave slope be the same for the incident and reflected wave. At the critical frequency where the wave slope becomes equal to the bottom slope the wavenumber, energy density, and shear are greatly amplified and shear instability and mixing are likely to occur. Energy and shear enhancement at the critical frequency have indeed been observed by Eriksen (1982) at a few sites. To obtain quantitative estimates Eriksen (1985) considered the reflection of a full spectrum of incident waves and calculated the energy flux that is redistributed in wavenumber space. A small fraction of this redistributed energy flux, if converted to mixing, would be sufficient to maintain an effective diapycnal diffusivity of magnitude 10^{-4} m^2 s^{-1} basinwide. To find out how much of the redistributed energy flux is actually available for mixing, Garrett and Gilbert (1988) argued that only waves reflected to high wavenumbers break and produce mixing. They therefore calculated the flux that is redistributed to wavenumbers beyond a critical wavenumber where the critical wavenumber is determined by the requirement that the spectrum up to this wavenumber has an inverse Richardson number of order one. These calculations support Eriksen's assertion and suggest that internal wave–induced boundary mixing is most efficient at low latitudes and steep slopes. In a second paper, Gilbert and Garrett (1989) investigate the effect of finite topography for a few idealized bottom shapes and conclude that mixing should be larger over locally convex than concave topography.

Most studies of internal wave scattering or reflection off particular bottom shapes are based on two papers by Baines (1971a,b) in which he reduced the problem to the solution of a Fredholm integral equation of the second kind. The study treats radiation conditions properly, finds backward- and forward-reflected waves, and has to distinguish between flat bumps with slopes smaller than and steep bumps with slopes larger than the wave slopes. Baines results are very general, except for their limitation to waves propagating in a two-dimensional vertical plane. A closed form solution of the Fredholm integral equation can, however, be obtained only for a few specific simple bottom profiles.

Analyses of the scattering or reflection process usually assume that the wave equation is linear. No non-

* Contribution Number 2770 from the School of Ocean and Earth Science Technology, University of Hawaii.

Corresponding author address: Dr. Peter Müller, University of Hawaii, Department of Oceanography, 1000 Pope Rd., Honolulu, HI 96822.

linear interactions among waves are considered. The interaction with the bottom topography enters through the kinematic boundary condition, which requires that the velocity normal to the topography is zero at the bottom. This condition is linear in the wave amplitude but nonlinear in the bottom height, as can be seen by expanding the condition at a reference depth. Waves can thus be superimposed; topographic components cannot. The scattering off an arbitrary bottom shape cannot be obtained by studying the reflection off its sinusoidal Fourier components. Such superposition becomes possible, however, when we restrict ourselves to topography for which the height is smaller than the vertical wavelength and the slope smaller than the wave slope. In this limit, the scattering of a full spectrum of incident waves off complex topography can be obtained by evaluating the scattering of a single wave off a single sinusoidal bottom Fourier component and summing over all incident waves and over all bottom Fourier components. This weak interaction limit will be taken in this paper.

The weak interaction limit was first applied by Cox and Sandstrom (1962) to the interaction with bottom topography using a vertical modal representation of the internal wave field. Later, Müller and Olbers (1975) derived the complete scattering integral in a vertical WKB approximation. Based on a rough order-of-magnitude estimate, Olbers and Pomphrey (1981) argued that bottom scattering is unimportant for typical ocean conditions, but Rubenstein (1988) found significant transfers in a detailed study. Rubenstein started from a formula given in Baines (1971a) and derived the probability that a wave is scattered from wavenumber $\mathbf{k}_1$ to wavenumber $\mathbf{k}_2$. Unfortunately, he interpreted this probability as a density in vertical wavenumber space, whereas it is a probability in horizontal wavenumber space, as can be seen from dimensional arguments. Also, the formula given in Müller and Olbers (1975) is not correct. A δ function and a numerical factor are missing. For these reasons, we derive the scattering integral by a systematic perturbation expansion of the governing equations and boundary condition. The derivation of the scattering integral is given in the first part of the paper (sections 2 through 4). Section 5 introduces the concept of the redistributed energy flux. In section 6 we then prove an H theorem, which states that scattering at random bottom topography always causes the wave field to approach an equilibrium spectrum where the energy flux is equipartitioned in horizontal wavenumber space. For red wave spectra this implies a transfer of the energy flux from low to high wavenumbers, a most significant result. To evaluate the rate at which the incoming energy flux is scattered to high wavenumbers, we have to specify both the spectrum of the incoming wave field and the spectrum of the bottom topography. Our estimates of the transfer are based on the Garrett and Munk 1976 internal wave spectral model (Desaubies 1976) and on Bell's (1975) bottom spectrum. Relevant features of these spectra are discussed in sections 7 and 8. The transfer rates as a function of frequency and horizontal wavenumber are given in sections 9 and 10 for the three- and two-dimensional cases, respectively. Section 11, finally, compares our scattering with Eriksen's reflection results.

Note that the scattering of internal waves at bottom topography is best analyzed in a representation where the frequency and the horizontal wavenumber vector are used as independent variables. The internal wave vertical wavenumber is then determined by the dispersion relation. This representation is most appropriate because scattering conserves the frequency and changes the horizontal wavenumber according to the simple resonance rule that incident wavenumber plus topographic wavenumber equals scattered wavenumber. Most intrinsic properties of the scattering are immediately apparent in the frequency–horizontal wavenumber representation but become obscured in any other representation.

2. Governing equations

To study the scattering of internal gravity waves at bottom topography, we consider a semi-infinite domain bounded by a bottom at $x_3 = h(x_1, x_2)$. The linearized equations for inviscid and incompressible motions in a uniformly stratified and rotating Boussinesq fluid are

$$\begin{aligned} \partial_t \mathbf{u} + f\mathbf{z} \times \mathbf{u} &= -\frac{1}{\rho_0}\nabla p - \frac{\rho g}{\rho_0}\mathbf{z} \\ \nabla \cdot \mathbf{u} &= 0 \\ \partial_t \rho + u_3 \partial_3 \tilde{\rho} &= 0 \end{aligned} \tag{2.1}$$

where the notation is standard. These equations have internal gravity wave solutions of the form

$$\mathbf{u}(\mathbf{x}, t) = a(\mathbf{k})\mathbf{U}(\mathbf{k}) \exp[i(\mathbf{k}\cdot\mathbf{x} - \omega t)] + \text{c.c.} \tag{2.2}$$

where $a(\mathbf{k})$ is the wave amplitude, $\mathbf{k} = (k_1, k_2, k_3)$ the wavenumber vector,

$$\begin{pmatrix} U_1(\mathbf{k}) \\ U_2(\mathbf{k}) \\ U_3(\mathbf{k}) \end{pmatrix} = \begin{pmatrix} \frac{k_3}{\alpha k}\left(k_1 + i\frac{f}{\omega}k_2\right) \\ \frac{k_3}{\alpha k}\left(k_2 - i\frac{f}{\omega}k_1\right) \\ -\frac{\alpha}{k} \end{pmatrix} \tag{2.3}$$

the polarization vector, and ω the frequency given by the dispersion relation

$$\omega = \Omega(\mathbf{k}) = +\left(\frac{N^2\alpha^2 + f^2\beta^2}{k^2}\right)^{1/2} \geqslant 0. \tag{2.4}$$

Here f and N are the Coriolis and Brunt–Väisälä frequency, respectively, and α, β, and k are the magnitudes

of the horizontal, vertical, and total wavenumber vector, respectively.

The interaction of the waves with the bottom topography arises through the kinematic boundary condition

$$u_3 - \mathbf{u}_h \cdot \nabla_h h = 0 \quad \text{at} \quad x_3 = h(x_1, x_2) \tag{2.5}$$

which states that the flow normal to the boundary is zero. Here $\mathbf{u}_h$ and ∇_h are the horizontal velocity and gradient operator, respectively. To evaluate the interaction we represent the bottom topography as a superposition of topographic Fourier components

$$h(x_1, x_2) = \int d^2\alpha b(\boldsymbol{\alpha}) e^{i\boldsymbol{\alpha}\cdot\mathbf{x}} \tag{2.6}$$

where $\boldsymbol{\alpha} = (k_1, k_2)$ is the horizontal wavenumber vector and $b(\boldsymbol{\alpha}) = b^*(-\boldsymbol{\alpha})$ are the topographic amplitudes. Similarly, we write the internal wave field as the sum of an incident wave field and a scattered wave field

$$\mathbf{u}(\mathbf{x}, t) = \int d^2\alpha \int_0^\infty dk_3 a_i(\mathbf{k})\mathbf{U}(\mathbf{k}) \times \exp[i(\mathbf{k}\cdot\mathbf{x} - \Omega(\mathbf{k})t)] + \text{c.c.} + \int d^2\alpha \int_{-\infty}^0 dk_3 \times a_s(\mathbf{k})\mathbf{U}(\mathbf{k}) \exp[i(\mathbf{k}\cdot\mathbf{x} - \Omega(\mathbf{k})t)] + \text{c.c.} \tag{2.7}$$

where $a_i(\mathbf{k})$ are the amplitudes of the incident and $a_s(\mathbf{k})$ the amplitudes of the scattered waves. The integration limits for the vertical wavenumber follow from the radiation condition. Incident waves must have a downward group velocity; scattered waves, an upward group velocity. Since the vertical group velocity is given by

$$v_3 = \frac{\partial\Omega}{\partial k_3} = -\frac{\omega^2 - f^2}{\omega}\frac{k_3}{k^2}, \tag{2.8}$$

the incident waves must have a positive vertical wavenumber and the scattered waves a negative vertical wavenumber, as in Eq. (2.7). The amplitudes of the incident waves, $a_i(\mathbf{k})$, are regarded as given. The amplitudes of the scattered waves, $a_s(\mathbf{k})$, must be calculated.

3. Perturbation expansion

The interaction between gravity waves and bottom topography via the kinematic boundary condition is nonlinear in the topographic amplitude. This becomes explicit once we expand the boundary condition

$$u_3 + h\partial_3 u_3 + \tfrac{1}{2}h^2\partial_3\partial_3 u_3 + \cdots - \mathbf{u}_h\cdot\nabla_h h - h\partial_3\mathbf{u}_h\cdot\nabla_h h - \cdots = 0 \tag{3.1}$$

at $x_3 = 0$, which becomes

$$u_3 - \nabla_h\cdot(h\mathbf{u}_h) - \nabla_h\left(\tfrac{1}{2}h^2\partial_3\mathbf{u}_h\right) - \cdots = 0 \quad \text{at} \quad x_3 = 0 \tag{3.2}$$

upon using the incompressibility condition. We now assume (i) that the height of the topography is smaller than the vertical scale β^{-1} of the waves, that is,

$$\epsilon_1 = h\beta \ll 1, \tag{3.3}$$

(ii) that the slope $\gamma = |\nabla_h\cdot h|$ of the topography is smaller than the slope $s = \alpha/\beta$ of the waves, that is,

$$\epsilon_2 = \gamma/s \ll 1, \tag{3.4}$$

and (iii) that the parameters ϵ_1 and ϵ_2 are of comparable magnitude ϵ. The expansion then represents an expansion with respect to the small parameter ϵ. The terms of order n in the topographic amplitude are of order ϵ^n. Note that the slope of internal waves is given by

$$s = \left(\frac{\omega^2 - f^2}{N^2 - \omega^2}\right)^{1/2}. \tag{3.5}$$

Hence, the expansion will break down for near-inertial oscillation where s approaches zero. A more quantitative discussion of the range of validity of our perturbation expansion will be given in section 8.

Next, we expand the amplitudes of the scattered waves with respect to ϵ

$$a_s(\mathbf{k}) = a_s^{(0)}(\mathbf{k}) + a_s^{(1)}(\mathbf{k}) + a_s^{(2)}(\mathbf{k}) + \cdots \tag{3.6}$$

where $a_s^{(n)}(\mathbf{k})$ is of order n in ϵ. The given amplitudes of the incident wave field are regarded as being of zeroth order. These amplitude expansions imply an expansion of the velocity field

$$\mathbf{u} = \mathbf{u}^{(0)} + \mathbf{u}^{(1)} + \mathbf{u}^{(2)} + \cdots \tag{3.7}$$

which we substitute into the kinematic boundary condition (3.2). The first three orders of the boundary condition are then given by

$$\begin{aligned} &\epsilon^0\text{: } u_3^{(0)} = 0 \\ &\epsilon^1\text{: } u_3^{(1)} = \nabla_h(h\mathbf{u}_h^{(0)}) \\ &\epsilon^2\text{: } u_3^{(2)} = \nabla_h(h\mathbf{u}_h^{(1)}) + \nabla_h\left(\tfrac{1}{2}h^2\mathbf{u}_h^{(0)}\right). \end{aligned} \tag{3.8}$$

Generally, the nth order of the boundary condition allows one to calculate the nth-order amplitude $a_s^{(n)}(\mathbf{k})$ in terms of lower-order and incident amplitudes. We will calculate the amplitudes of the scattered waves up to second order, using (3.8).

Upon substitution of the representation (2.7) and the expansion (3.6) the zeroth order of the boundary condition takes the explicit form

$$\int d^2\alpha \int_0^\infty dk_3 a_i(\mathbf{k}) U_3(\mathbf{k}) \exp[i(\boldsymbol{\alpha}\cdot\mathbf{x} - \Omega(\mathbf{k})t)] + \int d^2\alpha \int_{-\infty}^0 dk_3 a_s^{(0)}(\mathbf{k}) U_3(\mathbf{k}) \times \exp[i(\boldsymbol{\alpha}\cdot\mathbf{x} - \Omega(\mathbf{k})t)] = 0 \tag{3.9}$$

which implies

$$a_s^{(0)}(\boldsymbol{\alpha}, k_3) = -a_i(\boldsymbol{\alpha}, -k_3) \tag{3.10}$$

for $k_3 \leq 0$ since $U_3(\boldsymbol{\alpha}, -k_3) = U_3(\boldsymbol{\alpha}, k_3)$. To zeroth order, the scattered wave has the same horizontal wavenumber, the opposite vertical wavenumber, and hence the same frequency as the incident wave. The zeroth order is, of course, just the reflection at a flat bottom, $h = 0$. Additionally, we find the relations

$$\mathbf{u}_h^{(0)} = 2 \int d^2\alpha \int_0^\infty dk_3 a_i(\mathbf{k}) \times \mathbf{U}_h(\mathbf{k}) \exp[i(\boldsymbol{\alpha}\cdot\mathbf{x} - \Omega t)] + \text{c.c.} \quad (3.11)$$

and

$$\partial_3 \mathbf{u}_h^{(0)} = 0 \quad (3.12)$$

at $x_3 = 0$, which follow from $\mathbf{U}_h(\boldsymbol{\alpha}, -k_3) = -\mathbf{U}_h(\boldsymbol{\alpha}, k_3)$ and are needed in the following.

Note that incident (scattered) waves have positive (negative) vertical wavenumbers. Equation (3.10) is thus defined only for $k_3 \leq 0$. This restriction to permissible vertical wavenumbers will always be assumed in the following.

The first-order boundary condition takes the explicit form

$$\int d^2\alpha \int_{-\infty}^0 dk_3 a_s^{(1)}(\mathbf{k}) U_3(\mathbf{k}) \exp[i(\boldsymbol{\alpha}\cdot\mathbf{x} - \Omega(\mathbf{k})t)] = 2 \int d^2\alpha' \int_0^\infty dk_3' \int d^2\alpha'' i(\boldsymbol{\alpha}' + \boldsymbol{\alpha}'')\cdot \mathbf{U}_h(\mathbf{k}) a_i(\mathbf{k}') b(\boldsymbol{\alpha}'') \exp\{i[(\boldsymbol{\alpha}' + \boldsymbol{\alpha}'')\cdot\mathbf{x} - \Omega(\mathbf{k}')t]\} \quad (3.13)$$

which implies

$$\frac{a_s^{(1)}(\mathbf{k}) U_3(\mathbf{k})}{|v_3(\mathbf{k})|} = \int d^2\alpha' \int_0^\infty dk_3' \int d^2\alpha'' 2i\boldsymbol{\alpha}\cdot \mathbf{U}_h(\mathbf{k}') a_i(\mathbf{k}') b(\boldsymbol{\alpha}'') \delta(\boldsymbol{\alpha}' + \boldsymbol{\alpha}'' - \boldsymbol{\alpha}) \delta(\Omega(\mathbf{k}) - \Omega(\mathbf{k}')). \quad (3.14)$$

To first order, an incident internal wave $a_i(\mathbf{k}')$ of horizontal wavenumber $\boldsymbol{\alpha}'$, vertical wavenumber k_3', and frequency $\omega' = \Omega(\boldsymbol{\alpha}', k_3')$ interacts with a topographic Fourier component $b(\boldsymbol{\alpha}'')$ of horizontal wavenumber $\boldsymbol{\alpha}''$ to produce a scattered wave at horizontal wavenumber

$$\boldsymbol{\alpha} = \boldsymbol{\alpha}' + \boldsymbol{\alpha}'' \quad (3.15)$$

at frequency

$$\omega = \Omega(\boldsymbol{\alpha}, k_3) = \Omega(\boldsymbol{\alpha}', k_3') \quad (3.16)$$

and hence at vertical wavenumber

$$k_3 = -\frac{\alpha}{\alpha'} k_3'. \quad (3.17)$$

The efficiency of the scattering process is given by the scattering cross section

$$D = \frac{|v_3(\mathbf{k})|}{U_3(\mathbf{k})} 2i\boldsymbol{\alpha}\cdot \mathbf{U}_h(\mathbf{k}'). \quad (3.18)$$

The total effect is obtained by summing over all incident waves and topographic components that satisfy the resonance conditions (3.15) and (3.16).

Similarly, we obtain from the second-order boundary condition

$$\frac{a_s^{(2)}(\mathbf{k}) U_3(\mathbf{k})}{|v_3(\mathbf{k})|} = \int d^2\alpha' \int_{-\infty}^0 dk_3' \int d^2\alpha'' i\boldsymbol{\alpha}\cdot \mathbf{U}_h(\mathbf{k}') a_s^{(1)}(\mathbf{k}') b(\boldsymbol{\alpha}'') \delta(\boldsymbol{\alpha}' + \boldsymbol{\alpha}'' - \boldsymbol{\alpha}) \delta(\Omega(\mathbf{k}) - \Omega(\mathbf{k}')), \quad (3.19)$$

which describes the scattering of a scattered wave.

The expression (3.10), (3.14), and (3.19) for the amplitudes $a_s^{(0)}(\mathbf{k})$, $a_s^{(1)}(\mathbf{k})$, and $a_s^{(2)}(\mathbf{k})$ are the principal results of this section. They are obtained by a perturbation expansion of the problem with respect to the small parameter ϵ.

4. Energy spectra

We now assume that the amplitudes of the internal wave field are random realizations from a horizontally homogeneous and stationary ensemble. The wave amplitudes then satisfy the conditions

$$\langle a(\mathbf{k}) \rangle = 0 \quad (4.1)$$

$$\langle a(\mathbf{k}) a^*(\mathbf{k}') \rangle = \tfrac{1}{2} \delta(\mathbf{k} - \mathbf{k}') E(\mathbf{k}) \quad (4.2)$$

where angle brackets denote ensemble averages. The polarization vector (2.3) is normalized in such a way that $E(\mathbf{k})$ represents the total energy density spectrum, that is,

$$\int d^3k E(\mathbf{k}) = \tfrac{1}{2}(\langle \mathbf{u}\cdot\mathbf{u} \rangle + N^2 \langle \xi^2 \rangle). \quad (4.3)$$

Here ξ is the vertical displacement. For positive (negative) vertical wavenumbers $E(\mathbf{k})$ represents the spectrum of the incoming (scattered) waves.

Similarly, we assume

$$\langle b(\boldsymbol{\alpha}) \rangle = 0 \quad (4.4)$$

$$\langle b(\boldsymbol{\alpha}) b^*(\boldsymbol{\alpha}') \rangle = S(\boldsymbol{\alpha}) \delta(\boldsymbol{\alpha} - \boldsymbol{\alpha}') \quad (4.5)$$

where $S(\boldsymbol{\alpha})$ is the bottom spectrum normalized such that the variance of the topography is given by

$$\langle h^2 \rangle = \int d^2S(\boldsymbol{\alpha}). \tag{4.6}$$

We further assume that the amplitudes of the incident wave field and the amplitudes of the topography are uncorrelated.

To calculate the spectrum of the scattered wave field, we substitute the amplitude expansion (3.6) into the definition (4.2). In a straightforward manner we obtain an expansion of the spectrum of the scattered wave field. At lowest order we obtain

$$E_s^{00}(\boldsymbol{\alpha}, k_3) = E_i(\boldsymbol{\alpha}, -k_3) \tag{4.7}$$

upon substituting our solution (3.10) for $a_s^{(0)}(\mathbf{k})$. The scattered spectrum equals the incident wave spectrum at negative vertical wavenumbers. This result describes the reflection at a flat bottom $h = 0$. The superscript "00" is a reminder that this order arises from the product of two zeroth-order amplitudes.

At first order we obtain

$$E_s^{01}(\mathbf{k}) = 0 \tag{4.8}$$

since the incident waves and the bottom amplitudes are uncorrelated. At second order we find two terms. The first term arises from a product of two first-order amplitudes and is given by

$$E_s^{11}(\mathbf{k}) = \int d^2\alpha' \int_0^\infty dk_3' \times \int d^2\alpha'' T^s_{\mathbf{k},\mathbf{k}',\boldsymbol{\alpha}''} E_i(\mathbf{k}') S(\boldsymbol{\alpha}'') \tag{4.9}$$

upon substitution of our solution (3.14). The second term arises from two products of a zeroth- and a second-order amplitude and is given by

$$E_s^{02}(\mathbf{k}) = \int d^2\alpha' \int_0^\infty dk_3' \times \int d^2\alpha'' T^s_{\mathbf{k},\mathbf{k}',\boldsymbol{\alpha}''} E_i(\mathbf{k}) S(\boldsymbol{\alpha}'') \tag{4.10}$$

upon substitution of our solutions (3.10) and (3.19). The transfer function is given in both cases by

$$T^s_{\mathbf{k},\mathbf{k}',\boldsymbol{\alpha}''} = 4 \frac{\beta^2}{\alpha^2} \frac{1}{\alpha\alpha'} \left| \boldsymbol{\alpha} \cdot \boldsymbol{\alpha}' + i \frac{f}{\omega} \boldsymbol{\alpha} \cdot \mathbf{n}' \right|^2 \times \delta(\boldsymbol{\alpha}' + \boldsymbol{\alpha}'' - \boldsymbol{\alpha}) \delta\left(k_3' + \frac{\alpha'}{\alpha} k_3 \right) \tag{4.11}$$

with $\mathbf{n} = (k_2, -k_1)$. The first term, $E_s^{11}(\mathbf{k})$, is a gain term. It describes the gain of wave energy at wavenumber $(\boldsymbol{\alpha}, k_3)$ due to all incident waves $(\boldsymbol{\alpha}', k_3')$ that are scattered at bottom components $\boldsymbol{\alpha}''$ into wavenumber

$$\boldsymbol{\alpha} = \boldsymbol{\alpha}' + \boldsymbol{\alpha}'' \tag{4.12}$$

$$k_3 = -\frac{\alpha}{\alpha'} k_3'. \tag{4.13}$$

The second condition implies that the frequency of the incident and scattered waves are the same. This term is often written in the form

$$E_s^{11}(\mathbf{k}) = \int d^2\alpha' \int_0^\infty dk_3' p(\mathbf{k}, \mathbf{k}') E_i(\mathbf{k}') \tag{4.14}$$

with

$$p(\mathbf{k}, \mathbf{k}') = \int d^2\alpha'' T^s_{\mathbf{k},\mathbf{k}',\boldsymbol{\alpha}''} S(\boldsymbol{\alpha}'') \tag{4.15}$$

being interpreted as the probability that a wave of wavenumber $\mathbf{k}'$ is scattered into a wave of wavenumber $\mathbf{k}$.

The second term, E_s^{02}, is a loss term. It describes the loss of energy due to the fact that an incident wave $(\boldsymbol{\alpha}, -k_3)$ that would have appeared at wavenumber $(\boldsymbol{\alpha}, k_3)$ upon reflection is scattered to a different wavenumber. This term is often written as

$$E_s^{02}(\mathbf{k}) = -\gamma(\mathbf{k}) E_i(\mathbf{k}) \tag{4.16}$$

with the "damping" coefficient

$$\gamma(\mathbf{k}) = \int d^2\alpha' \int_0^\infty dk_3' p(\mathbf{k}, \mathbf{k}'). \tag{4.17}$$

The terms E_s^{11} and E_s^{02} are of the same order. One must go to the second order in the amplitude expansion to obtain the first nontrivial correction to the scattered spectrum

$$\begin{aligned} E_s(\boldsymbol{\alpha}, k_3) - E_i(\boldsymbol{\alpha}, -k_3) &= E_s^{11}(\mathbf{k}) + E_s^{02}(\mathbf{k}) + O(\epsilon^3) \\ &= \int d^2\alpha' \int_0^\infty dk_3' \int d^2\alpha'' T^s_{\mathbf{k},\mathbf{k}',\boldsymbol{\alpha}''} S(\boldsymbol{\alpha}'') \\ &\quad \times [E_i(\mathbf{k}') - E_i(\mathbf{k})] + O(\epsilon^3). \end{aligned} \tag{4.18}$$

Equation (4.18) is the principal result of this section. Note that it differs by an algebraic factor and a δ function from the formula given in Müller and Olbers (1975).

Equation (4.18) can be used to calculate the energy density E_s of the scattered wave field when the energy density E_i of the incident wave field is given. This is the point of view we will take in this paper. Equation (4.18) can also be used as a lower boundary condition for the radiation balance equation. The radiation balance equation describes the slow evolution (in a WKB sense) of the energy density spectrum due to propagation, refraction, and interaction processes. In terms of the action density spectrum $A(\mathbf{k}, \mathbf{x}, t)$, which is the energy density spectrum divided by the intrinsic frequency, the radiation balance equation takes the suggestive form (Müller and Olbers 1975)

$$\partial_t A + \mathbf{v} \cdot \nabla A + \mathbf{r} \cdot \nabla_{\mathbf{k}} A = S \tag{4.19}$$

where $\mathbf{v}$ is the group velocity, $\mathbf{r}$ the rate of refraction, and S the source function representing all the inter-

action processes that generate, transfer, and dissipate action. If the source function is zero, action is conserved. The radiation balance equation must be augmented by radiation conditions at the boundaries that determine the action or energy flux through the boundary. At the bottom such radiation conditions take the general form

$$v_3(\boldsymbol{a}, k_3)E(\boldsymbol{a}, k_3) + v_3(\boldsymbol{a}, -k_3)E(\boldsymbol{a}, -k_3) = D(\boldsymbol{a}, k_3) \quad \text{at} \quad x_3 = 0 \quad (4.20)$$

where $D(\boldsymbol{a}, k_3)$ is the net flux of energy through the boundary. For bottom scattering the net energy flux through the bottom is given by

$$\begin{aligned} D_s(\boldsymbol{a}, k_3) &= F_s(\boldsymbol{a}, k_3) + F_i(\boldsymbol{a}, -k_3) \\ &= v_3(\boldsymbol{a}, k_3)[E(\boldsymbol{a}, k_3) - E_i(\boldsymbol{a}, -k_3)] \\ &= v_3(\mathbf{k})[E_s^{11}(\mathbf{k}) + E_s^{02}(\mathbf{k})] + O(\epsilon^3), \end{aligned} \quad (4.21)$$

where F_s is the energy flux of the scattered waves and F_i the energy flux of the incident waves.

5. The redistributed energy flux

In the derivation of the scattering integral (4.18) we have followed the recipes of Müller and Olbers (1975); especially, we have used the three components of the wavenumber vector as independent variables and inferred the frequency from the dispersion relation (2.4). For the actual discussion and evaluation of the scattering process, it is much more convenient to change from the $\mathbf{k} = \{\boldsymbol{a}, k_3\}$ representation to the $\{\boldsymbol{a}, \omega, \mu\}$ representation where $\mu = \text{sgn}(k_3)$ and $\omega > 0$ and to infer the vertical wavenumber from

$$k_3 = \text{sgn}(k_3)\left(\frac{N^2 - \omega^2}{\omega^2 - f^2}\right)^{1/2}\alpha. \quad (5.1)$$

Incident waves have $\mu = +1$ and scattered waves $\mu = -1$. This representation is more convenient since bottom scattering does not change the frequency.

In $\{\boldsymbol{a}, \omega\}$ space, the net flux of energy through the bottom is given by

$$\begin{aligned} D_s(\boldsymbol{a}, \omega) &= F_s(\boldsymbol{a}, \omega) + F_i(\boldsymbol{a}, \omega) \\ &= \int d^2\alpha' \int d^2\alpha'' T^s_{\boldsymbol{a},\boldsymbol{a}',\boldsymbol{a}''}(\omega)S(\boldsymbol{a}'') \\ &\quad \times \left[E_i(\boldsymbol{a}', \omega)\frac{V(\omega)}{\alpha'} - E_i(\boldsymbol{a}, \omega)\frac{V(\omega)}{\alpha}\right] \end{aligned} \quad (5.2)$$

where

$$\begin{aligned} T^s_{\boldsymbol{a},\boldsymbol{a}',\boldsymbol{a}''}(\omega) &= 2\frac{N^2 - \omega^2}{\omega^2 - f^2}\frac{1}{\alpha\alpha'} \\ &\quad \times \left|\boldsymbol{a}\cdot\boldsymbol{a}' + i\frac{f}{\omega}\boldsymbol{a}\cdot\mathbf{n}'\right|^2 \delta(\boldsymbol{a}' + \boldsymbol{a}'' - \boldsymbol{a}). \end{aligned} \quad (5.3)$$

The function

$$V(\omega) = \frac{(\omega^2 - f^2)^{3/2}(N^2 - \omega^2)^{1/2}}{\omega(N^2 - f^2)} \quad (5.4)$$

arises because the vertical group velocity is given by

$$v_3(\alpha, \omega, \mu) = -\mu\frac{V(\omega)}{\alpha} \quad (5.5)$$

in the $\{\boldsymbol{a}, \omega, \mu\}$ representation; $D_s(\boldsymbol{a}, \omega)$ is the net energy flux through the bottom at horizontal wavenumber $\boldsymbol{a}$ and frequency ω. The flux is due to an incoming wave $\{\boldsymbol{a}, \omega, \mu = +1\}$ and a scattered wave $\{\boldsymbol{a}, \omega, \mu = -1\}$. Since the transfer function $T^s_{\boldsymbol{a},\boldsymbol{a}',\boldsymbol{a}''}(\omega)$ is symmetric in $\boldsymbol{a}$ and $\boldsymbol{a}'$, whereas the expression in braces is antisymmetric in $\boldsymbol{a}$ and $\boldsymbol{a}'$, we find

$$\int d^2\alpha D_s(\boldsymbol{a}, \omega) = 0. \quad (5.6)$$

The integrated energy flux through the bottom vanishes for each frequency. For each frequency, bottom scattering only redistributes the incoming energy flux in horizontal wavenumber space.

Note that throughout this paper, spectra are always normalized such that integration over their arguments gives the variance. Therefore,

$$\int_f^N d\omega D_s(\boldsymbol{a}, \omega) = \int_{-\infty}^0 dk_3 D_s(\boldsymbol{a}, k_3) \quad (5.7)$$

$$\int_f^N d\omega E(\boldsymbol{a}, \omega) = \int_{-\infty}^0 dk_3 E(\boldsymbol{a}, k_3) \quad (5.8)$$

in (5.2).

6. Equilibrium solution

It immediately follows from Eq. (5.2) that $D_s(\boldsymbol{a}, \omega) = 0$ if, and only if, the incident energy density spectrum is of the form

$$E_i(\boldsymbol{a}, \omega) = f(\omega)\frac{\alpha}{V(\omega)} \quad (6.1)$$

where f is a positive but otherwise arbitrary function of frequency. This arbitrary function reflects the fact that bottom scattering does not change the frequency of the incoming waves. Bottom scattering does not spread information between frequencies. All frequencies are independent. For the equilibrium solution the incoming energy flux

$$F_i(\boldsymbol{a}, \omega) = v_3(\boldsymbol{a}, \omega, \mu = +1)E_i(\boldsymbol{a}, \omega) = -f(\omega) \quad (6.2)$$

is equipartitioned over all horizontal wavenumbers, a result that suggests a statistical mechanics interpretation. Indeed, the equilibrium solution (6.1) is the solution that maximizes the entropy functional

$$S(\omega) = \int d^2\alpha \ln E_i(\boldsymbol{a}, \omega) \quad (6.3)$$

subject to the constraint that the integrated incident energy flux is a constant

$$\int d^2\alpha E_i(\boldsymbol{\alpha}, \omega) \frac{V(\omega)}{\alpha} = \text{const.} \tag{6.4}$$

This can be seen by varying the entropy functional with respect to E_i and representing the constraint by Lagrange multipliers $\lambda(\omega) = f^{-1}(\omega)$

$$\delta S = \int d^2\alpha \left\{ \frac{1}{E_i(\boldsymbol{\alpha}, \omega)} - \lambda(\omega) \frac{V(\omega)}{\alpha} \right\} \delta E_i(\boldsymbol{\alpha}, \omega)$$

$$\delta^2 S = -\int d^2\alpha \frac{1}{E_i^2(\boldsymbol{\alpha}, \omega)} (\delta E_i(\boldsymbol{\alpha}, \omega))^2 \leq 0. \tag{6.5}$$

Furthermore, we can prove an H theorem. Bottom scattering increases the entropy

$$\begin{aligned}
\Delta S &\approx \int d^2\alpha \ln \frac{E_s(\boldsymbol{\alpha}, \omega)}{E_i(\boldsymbol{\alpha}, \omega)} \\
&= \int d^2\alpha \ln\left(1 + \frac{E_s(\boldsymbol{\alpha}, \omega) - E_i(\boldsymbol{\alpha}, \omega)}{E_i(\boldsymbol{\alpha}, \omega)}\right) \\
&\approx \int d^2\alpha \frac{E_s(\boldsymbol{\alpha}, \omega) - E_i(\boldsymbol{\alpha}, \omega)}{E_i(\boldsymbol{\alpha}, \omega)} \\
&= \int d^2\alpha \int d^2\alpha' \int d^2\alpha'' T^s_{\boldsymbol{\alpha},\boldsymbol{\alpha}',\boldsymbol{\alpha}''}(\omega) S(\boldsymbol{\alpha}'') \\
&\quad \times \frac{\alpha}{E_i(\boldsymbol{\alpha}, \omega)} \left\{ \frac{E_i(\boldsymbol{\alpha}', \omega)}{\alpha'} - \frac{E_i(\boldsymbol{\alpha}, \omega)}{\alpha} \right\} \\
&= \int d^2\alpha \int d^2\alpha' \int d^2\alpha'' \frac{1}{\alpha\alpha'} T^s_{\boldsymbol{\alpha},\boldsymbol{\alpha}',\boldsymbol{\alpha}''}(\omega) S(\boldsymbol{\alpha}'') \\
&\quad \times E_i(\boldsymbol{\alpha}, \omega) E_i(\boldsymbol{\alpha}', \omega) \\
&\quad \times \frac{1}{2} \left\{ \frac{\alpha}{E_i(\boldsymbol{\alpha}, \omega)} - \frac{\alpha'}{E_i(\alpha', \omega)} \right\}^2 \geq 0.
\end{aligned} \tag{6.6}$$

Therefore, bottom scattering will cause the energy or energy flux spectra to approach the equilibrium forms. Of course, the equilibrium spectra diverge at high wavenumbers, as is expected for a system with an infinite number of degrees of freedom. Nevertheless, the H theorem implies that the general trend of bottom scattering must be a transfer of energy from low to high horizontal wavenumbers. To evaluate the rate at which the incoming energy is scattered to high wavenumbers, we have to specify both the spectrum of the incoming internal wave field and the spectrum of the bottom topography. We do this in the next two sections.

7. The Garrett and Munk spectral model

Spectral models of the oceanic internal gravity wave field have been discussed at length in the literature (e.g., Olbers 1983). Here we list, for definiteness, the version that we will apply and point out the features that are relevant for the bottom-scattering problem. Since we have formulated the problem in terms of a continuous vertical wavenumber, we use the version generally referred to as the GM76 spectral model (Desaubies 1976). It is essentially equivalent to the Cairns and Williams (1976) and Munk (1981) versions, which are, however, formulated in terms of discrete vertical mode numbers.

The GM76 model assumes that the distribution of energy is horizontally isotropic and that the energy spectrum per unit mass as a function of frequency and horizontal wavenumber is given in the separable form

$$E(\omega, \alpha) = b^2 N N_0 E_0 B(\omega) \frac{A(\alpha/\alpha_*)}{\alpha_*} \tag{7.1}$$

where

$$B(\omega) = \frac{2}{\pi} \frac{f}{\omega} (\omega^2 - f^2)^{-1/2} \tag{7.2}$$

$$A(\lambda) = \frac{2}{\pi} (1 + \lambda^2)^{-1} \tag{7.3}$$

and $N_0 = 5.2 \times 10^{-3}\ \text{s}^{-1}$, $E_0 = 6 \times 10^{-5}$, and $b = 1.3 \times 10^3$ m. The bandwidth is given by

$$\alpha_*(\omega) = \left(\frac{\omega^2 - f^2}{N^2 - \omega^2} \right)^{1/2} \beta_* \tag{7.4}$$

where

$$\beta_* = \frac{\pi}{b} \left(\frac{N^2 - \omega^2}{N_0^2 - \omega^2} \right)^{1/2} j_*. \tag{7.5}$$

Here $j_* = 3$ is the frequency-independent equivalent mode-number bandwidth. The spectrum also includes a high wavenumber cutoff

$$\alpha_{uc}(\omega) = \left(\frac{\omega^2 - f^2}{N^2 - \omega^2} \right)^{1/2} \beta_{uc} \tag{7.6}$$

where $\beta_{uc} = 2\pi/10\ \text{m}^{-1}$ is a frequency-independent vertical cutoff wavenumber. In applications we will always assume $N = 0.4$ cph (deep ocean) and $f = 0.042$ cph (midlatitude, 30°) as standard parameters.

The vertical energy flux, $F_i(\boldsymbol{\alpha}, \omega)$, has a nonintegrable singularity proportional to α^{-1} as α approaches zero. To remove this singularity we introduce a lower cutoff wavenumber, α_{lc}, such that the integrated energy flux is equal to the flux obtained in a discrete modal representation (Munk 1981). We therefore require

$$\int_{\alpha_{lc}}^{\infty} d\alpha F_i(\omega, \alpha) = \sum_{j=1}^{\infty} F_i(\omega, j) \tag{7.7}$$

which implies

$$\alpha_{lc}(\omega) = \left(\frac{\omega^2 - f^2}{N_0^2 - \omega^2} \right)^{1/2} \frac{\pi}{b} j_{lc} \tag{7.8}$$

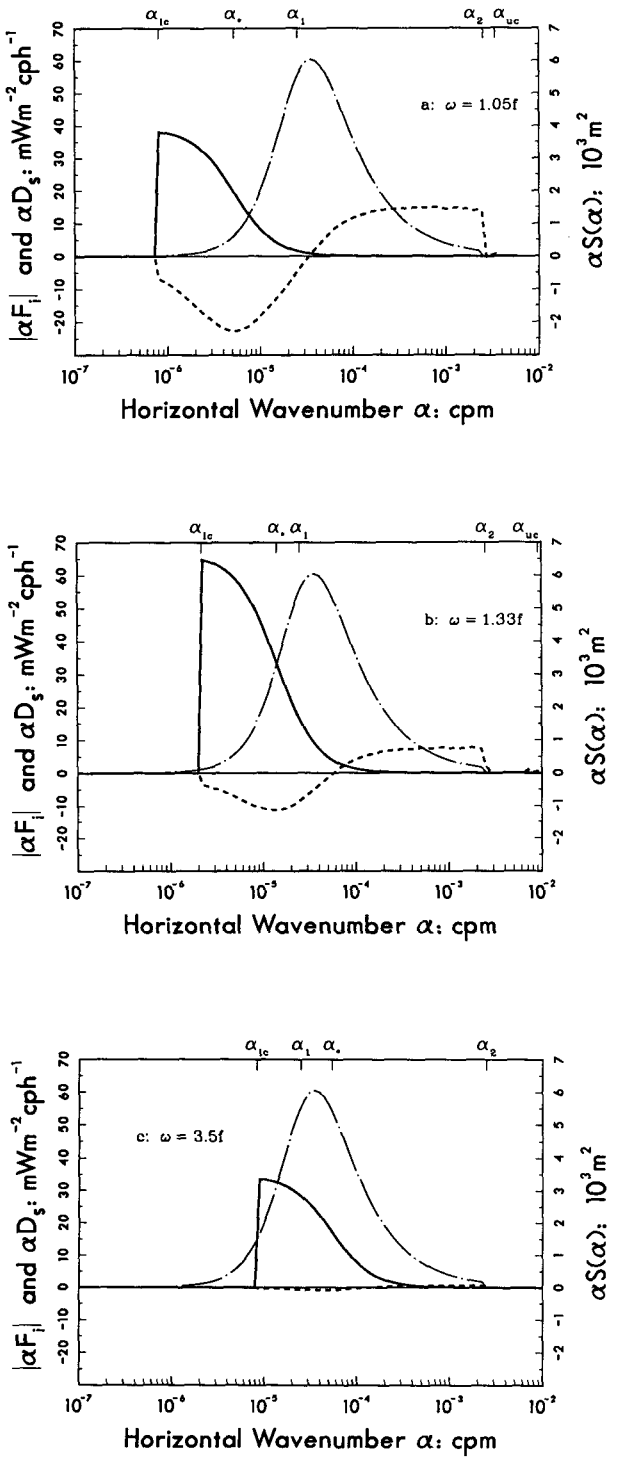

FIG. 1. Incident energy flux $|F_i(\alpha, \omega)|$ (solid line), bottom spectrum $S(\alpha)$ (dash-dotted line), and redistributed energy flux $D_s(\alpha, \omega)$ (dashed line) as a function of horizontal wavenumber for three different frequencies. The representation is variance conserving. The wavenumbers α_1 and α_2 are the bandwidth and the high wavenumber cutoff of the topographic spectrum, respectively. The wavenumbers α_{lc}, α_*, and α_{uc} are the low wavenumber cutoff, the bandwidth, and the high wavenumber cutoff of the incident internal wave spectrum, respectively.

with $j_{lc} \approx 0.5$, a sensible result. The incident energy flux $F_i(\boldsymbol{\alpha}, \omega)$ as a function of α for three values of ω is shown as part of Fig. 1. The integrated fluxes $F_i(\alpha) = \int d\omega F_i(\boldsymbol{\alpha}, \omega)$ and $F_i(\omega) = \int d\alpha F_i(\boldsymbol{\alpha}, \omega)$ are shown as part of Figs. 3 and 4. The total incident energy flux, integrated over all horizontal wavenumbers and all frequencies, is $F_i = 17.6$ mW m^{-2} for our standard parameters.

8. Bell's bottom spectrum

The statistical representation of seafloor topography meets with problems related to inhomogeneity and the presence of deterministic features. Nevertheless, spectral representation captures most of the relevant properties of topography for our scattering problem. Specifically, we will apply the bottom spectrum advocated by Bell (1975), which is of the form

$$S(\alpha) = AC(\alpha). \tag{8.1}$$

Here A is the height variance

$$A = \langle h^2 \rangle = (125 \text{ m})^2 \tag{8.2}$$

and $C(\alpha)$ the normalized wavenumber distribution

$$C(\alpha) = \begin{cases} \dfrac{\alpha\alpha_1}{(\alpha^2 + \alpha_1^2)^{3/2}}, & \text{for } \alpha < \alpha_2 \\ 0, & \text{for } \alpha > \alpha_2. \end{cases} \tag{8.3}$$

The bandwidth α_1 and the cutoff wavenumber α_2 have the values

$$\alpha_1 = 2\pi \cdot 2.5 \times 10^{-5} \text{ m}^{-1} \tag{8.4}$$

and

$$\alpha_2 = 2\pi \cdot 2.5 \times 10^{-3} \text{ m}^{-1}, \tag{8.5}$$

respectively.

Having specified the spectra of the incoming internal wave field and of the bottom topography, we can now examine the magnitudes of our expansion parameters $\epsilon_1 = h/\beta$ and $\epsilon_2 = \gamma/s$ in the root-mean-square sense. The GM spectrum implies a vertical wavenumber variance of

$$\langle \beta^2 \rangle = \frac{\int d\alpha E(\omega, \alpha)\beta^2}{\int d\alpha E(\omega, \alpha)} \approx \beta_* \beta_{uc} \approx \left(\frac{2\pi}{100 \text{ m}}\right)^2 \frac{N}{N_0}. \tag{8.6}$$

This, together with (8.2), implies

$$\epsilon_1 = 2\pi \frac{125}{100} \left(\frac{N}{N_0}\right)^{1/2} \tag{8.7}$$

which is of order 1 for the deep ocean where $N/N_0 \approx 10^{-1}$. Similarly, Bell's spectrum implies a slope variance of

$$\gamma^2 = \langle (\partial_1 h)^2 + (\partial_2 h)^2 \rangle$$

$$= \int d\alpha S(\alpha)\alpha^2 = A\alpha_1\alpha_2 \approx (0.2)^2 \quad (8.8)$$

and hence

$$\epsilon_2 = 0.2\left(\frac{N^2 - \omega^2}{\omega^2 - f^2}\right)^{1/2} \quad (8.9)$$

which is larger than 1 for $\omega < 2f$. For typical ocean conditions our perturbation expansion is only marginally valid and breaks down for near-inertial oscillations. Our results will, however, be qualitatively correct since the approach to the equipartitioned spectrum is a general tendency not limited to weak interactions. Also, the approach to equilibrium is generally faster the larger the nonlinearities are. Hence, our results can be expected to represent a lower bound.

9. Transfer rates

The evaluation of the redistributed energy flux (5.2) for the Garrett and Munk internal wave spectrum and for Bell's bottom spectrum is straightforward, though the integral has to be evaluated numerically. The result is presented in Fig. 1, which shows the incident energy flux $F_i(\alpha, \omega)$, the bottom spectrum $S(\alpha)$, and the redistributed energy flux $D_s(\alpha, \omega)$ as a function of α for three different frequencies. The representation is variance conserving. Bottom scattering redistributes the energy flux from low to high wavenumbers. There is no net flux through the bottom. The area of the negative lobe equals the area of the positive lobe. The redistribution is more efficient at low than at high frequencies.

A contour plot of $D_s(\alpha, \omega)$ in (α, ω) space is shown in Fig. 2, again showing the main features: redistribution from low to high wavenumbers, most efficiently at low frequencies. The total redistributed energy flux (the total energy flux in the positive or negative lobe) is

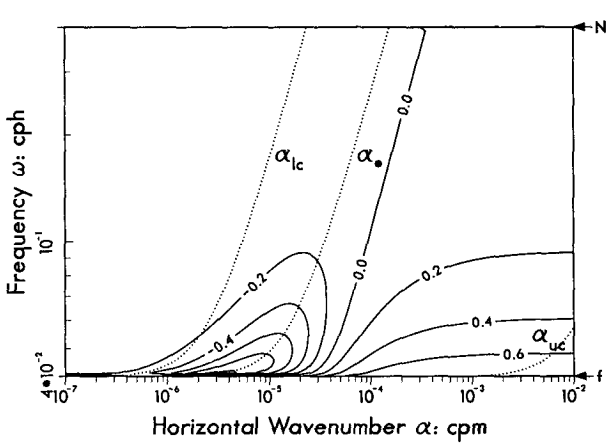

FIG. 2. Contours of redistributed energy flux $D_s(\alpha, \omega)$ as a function of horizontal wavenumber and frequency in a variance-conserving representation. The dotted lines are the low wavenumber cutoff $\alpha_{lc}(\omega)$, the bandwidth $\alpha_*(\omega)$ and high wavenumber cutoff $\alpha_{uc}(\omega)$, respectively.

$$D_s^+ = \frac{1}{2}\int d\omega \int d\alpha |D_s(\alpha, \omega)| \approx 1.20 \text{ mW m}^{-2} \quad (9.1)$$

for our standard parameters. This is about 6.8% of the total incoming energy flux of 17.6 mW m^{-2}, a significant fraction.

Closer inspection of the transfer function and of the scales of the bottom and internal wave spectrum reveals that waves scattered to high wavenumbers come predominantly from low wavenumbers. In the gain term we can hence assume $\alpha' \ll \alpha_1, \alpha''$, and

$$E_i(\boldsymbol{\alpha}', \omega) = E(\omega)\delta(\boldsymbol{\alpha}'). \quad (9.2)$$

The gain term then becomes

$$D_s^{11}(\boldsymbol{\alpha}, \omega) \approx 2\frac{N^2 - \omega^2}{\omega^2 - f^2}\frac{1}{2}\frac{\omega^2 + f^2}{\omega^2}\frac{V(\omega)}{\alpha}E(\omega)\alpha^2 S(\boldsymbol{\alpha}) \quad (9.3)$$

and is proportional to the incident energy flux times the expansion parameter ϵ_2^2. Similarly, we can assume $\alpha \ll \alpha', \alpha''$ in the loss term and obtain

$$D_s^{02}(\boldsymbol{\alpha}, \omega) \approx -2\frac{N^2 - \omega^2}{\omega^2 - f^2}\frac{1}{2}\frac{\omega^2 + f^2}{\omega^2}V(\omega)E(\boldsymbol{\alpha}, \omega)C \quad (9.4)$$

where

$$C = \int d^2\alpha\alpha S(\boldsymbol{\alpha}) = A\alpha_1\left\{\ln\frac{2\alpha_2}{\alpha_1} - 1\right\}. \quad (9.5)$$

The approximations (9.3) and (9.4) are indistinguishable from the numerically evaluated solution when plotted in Fig. 1. They are particularly useful to establish the dependence of the redistributed energy flux on the various parameters that enter the problem.

Integration of (9.3) and (9.4) over horizontal wavenumber α yields

$$D_s^{11}(\omega) = \int d^2\alpha D_s^{11}(\boldsymbol{\alpha}, \omega) = 2\frac{N^2 - \omega^2}{\omega^2 - f^2}\frac{1}{2}\frac{\omega^2 + f^2}{\omega^2}V(\omega)E(\omega)C \quad (9.6)$$

and

$$D_s^{02}(\omega) = \int d^2\alpha D_s^{02}(\boldsymbol{\alpha}, \omega) = -D_s^{11}(\omega). \quad (9.7)$$

The approximations of the transfer integral are hence self-consistent. A further integration over ω yields the total flux

$$D_s^{11} = \int d\omega \int d^2\alpha D_s^{11}(\boldsymbol{a}, \omega)$$

$$= 2C\frac{1}{2}b^2N^2N_0E_0\frac{2}{\pi}\frac{4}{3} \quad (9.8)$$

which depends linearly on N^2, A, and α_1 and logarithmically on α_2. For our standard parameters we find $D_s^{11} \approx 3.3$ mW m^{-2}, which is larger than the redistributed energy flux $D_s^+ \approx 1.20$ mW m^{-2} since $D_s^{11}(\boldsymbol{a}, \omega)$ and $D_s^{02}(\boldsymbol{a}, \omega)$ cancel in part of the $(\boldsymbol{a}, \omega)$ plane.

One can construct various integrated measures of the redistributed energy flux. One such measure is

$$D_s^+(\omega) = \frac{1}{2}\int d^2\alpha |D_s(\boldsymbol{a}, \omega)| \quad (9.9)$$

which integrates only over the positive (or negative) lobe of $D_s(\boldsymbol{a}, \omega)$. The function $D_s^+(\omega)$ is shown in Fig. 3 and again shows that most of the redistribution occurs at low frequencies. Of course $\int d\omega D_s^+(\omega) = D_s^+ = 1.20$ mW m^{-2}. Though one could construct a similar measure in wavenumber space, we show in Fig. 4 the integrated redistributed energy flux

$$D_s(\alpha) = \int d\omega D_s(\alpha, \omega) \quad (9.10)$$

which characterizes the actual redistribution in horizontal wavenumber space. Here $D_s(\alpha)$ is smaller than $D_s^+(\alpha)$ since during frequency integration cancellations of positive and negative contributions occur. The zero crossings of $D_s(\alpha, \omega)$ depend on frequency and wavenumber (see Fig. 2). The effect is, however, small. The total energy flux in the positive (or negative) lobe of Fig. 4 is 1.14 mW m^{-2}, only slightly smaller than the total redistributed energy flux $D_s^+ \approx 1.20$ mW m^{-2}.

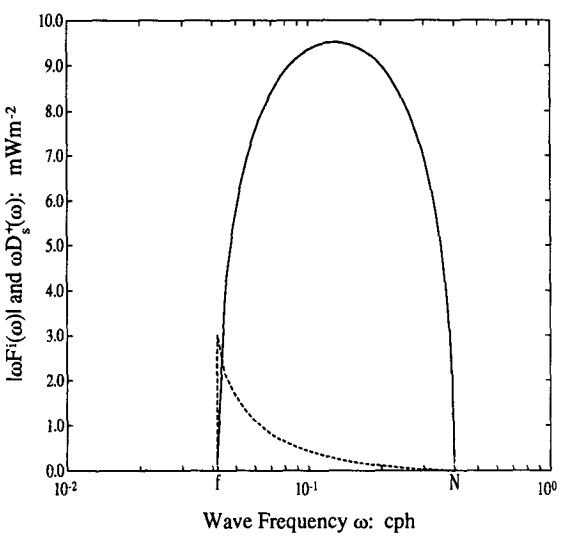

FIG. 3. Incident energy flux $|F_i(\omega)|$ (solid line) and redistributed energy flux $D_s^+(\omega)$ (dashed line) as a function of frequency in a variance-conserving representation.

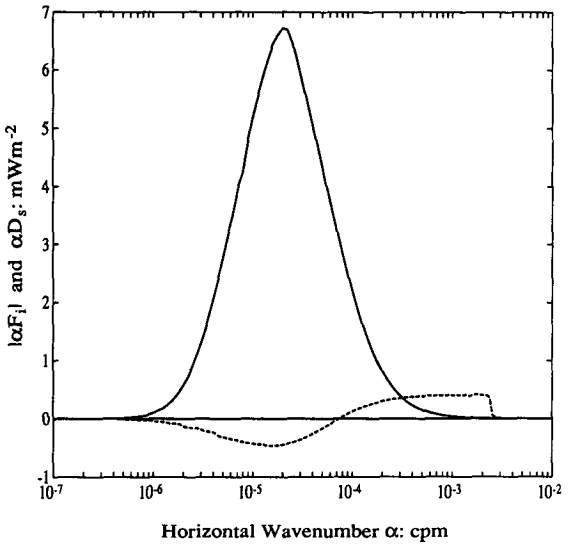

FIG. 4. Incident energy flux $|F_i(\alpha)|$ (solid line) and redistributed energy flux $D_s(\alpha)$ (dashed line) as a function of horizontal wavenumber in a variance-conserving representation.

10. Two-dimensional limit

Most of the previous investigations of the scattering problem are based on the papers by Baines (1971a,b), who studied the scattering process under the assumption that both wave motions and bottom topography are independent of the x_2 coordinate. This two-dimensional limit can be obtained from our three-dimensional analysis by setting

$$E(\omega, \boldsymbol{a}) = E(\omega, \alpha_1)\delta(\alpha_2) \quad (10.1)$$

$$S(\boldsymbol{a}) = S(\alpha_1)\delta(\alpha_2) \quad (10.2)$$

in the scattering integral (5.2). For symmetric $E(\omega, \alpha_1)$ we then obtain

$$D_s^{2D}(\alpha_1, \omega)$$

$$= \int_{-\infty}^{\infty} d\alpha_1' P(\alpha_1, \alpha_1')[F_i(\alpha_1', \omega) - F_i(\alpha_1, \omega)] \quad (10.3)$$

where

$$P(\alpha_1, \alpha_1') = 2\frac{N^2 - \omega^2}{\omega^2 - f^2}|\alpha_1\alpha_1'|S(\alpha_1 - \alpha_1')$$

$$= 2|k_3k_3'|[S(\alpha_1 - \alpha_1') + S(\alpha_1 + \alpha_1')] \quad (10.4)$$

is the probability density that a wave of wavenumber α_1' is scattered into wavenumber α_1. This expression for $P(\alpha_1, \alpha_1')$ is identical to the one of Rubenstein (1988), except that he interpreted it as a probability density with respect to vertical wavenumber, whereas

it is a density with respect to horizontal wavenumber, as can be seen by its dimension. Thus, our results differ by a factor of

$$s = \left[\frac{\omega^2 - f^2}{N^2 - \omega^2}\right]^{1/2}$$

from Rubenstein's results. This factor does not affect the qualitative behavior of the flux redistribution but its magnitude. Our redistributed energy flux is smaller than the one calculated by Rubenstein.

The redistributed energy flux (10.3) for the two-dimensional geometry does not differ much from the three-dimensional result. The total redistributed energy flux is 1.07 mW m^{-2}, about 10% smaller.

11. Comparison with reflection

Reflection off a sloping bottom also leads to a redistribution of the energy flux in wavenumber space. To compare the reflection and scattering process, we consider without loss of generality a uniformly sloping bottom in x_1 direction, $x_3 = \gamma x_1$, where $\gamma = \tan\varphi_0$ is the slope and $0 \leq \varphi_0 < \pi/2$. The normal vector $\mathbf{n} = (-\gamma, 0, +1)$ is assumed to point into the fluid. Reflection requires that the velocity of the incident and reflected wave normal to the slope is identically zero on the slope. This implies the reflection laws

$$\Omega(\mathbf{k}^r) = \Omega(\mathbf{k}^i) \tag{11.1}$$

$$k_2{}^r = k_2{}^i \tag{11.2}$$

$$k_1{}^r + \gamma k_3{}^r = k_1{}^i + \gamma k_3{}^i \tag{11.3}$$

which state that the frequency and the wavenumber parallel to the bottom do not change upon reflection. The superscripts i and r stand for incident and reflected, respectively.

The three-dimensional reflection laws have been analyzed by Eriksen (1982, 1985) and turn out to be algebraically quite complex. For comparison with the scattering process we consider, without loss of essential physics, the simpler two-dimensional case; that is, we assume $k_2{}^i = k_2{}^r = 0$. The reflection law can then easily be visualized in the (k_1, k_3) plane of Fig. 5, which shows the frequency cone

$$\tan^2\theta = \frac{k_3{}^2}{k_1{}^2} = \frac{N^2 - \omega^2}{\omega^2 - f^2} \tag{11.4}$$

for a particular frequency. Constancy of frequency and alongslope wavenumber require that the incident and reflected wavenumbers lie on the intersections of the frequency cone with lines perpendicular to the bottom slope. A wave is an incident wave when its group velocity is toward the slope, $\mathbf{n}\cdot\mathbf{v} < 0$, and a reflected wave when its group velocity is away from the slope, $\mathbf{n}\cdot\mathbf{v} > 0$. Figure 6 shows the regions of permissible incident wavenumbers in (k_1, k_3) space and the regions to which the incident wavenumbers are reflected. A particular role in this diagram is played by the frequency cone that has a slope perpendicular to the bottom slope, $\tan^2\theta = \cot^2\varphi_0$, which is the cone of the critical frequency

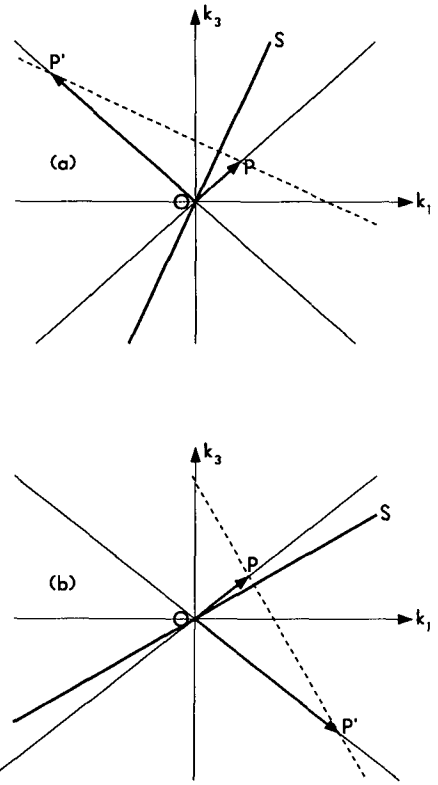

FIG. 5. Schematic diagram showing the two-dimensional reflection laws in the horizontal–vertical wavenumber plane. The heavy solid straight line represents the bottom slope, the light solid lines represent the frequency cone. The dashed line is perpendicular to the bottom slope. An incoming wave with wavenumber $\overrightarrow{OP}$ is therefore reflected to a wave with wavenumber $\overrightarrow{OP'}$. If the slope of dashed line is smaller than the slope of the frequency cone, the reflection is subcritical as in (a). If the slope of the dashed line is larger than the slope of the frequency cone, the reflection is supercritical as in (b).

$$\omega_c{}^2 = N^2 \sin^2\varphi_0 + f^2 \cos^2\varphi_0. \tag{11.5}$$

In this case $\mathbf{v}\cdot\mathbf{n} = 0$ for either the incident or reflected wave. The behavior of the reflection process is different for supercritical, $\omega > \omega_c$, and subcritical, $\omega < \omega_c$, frequencies. The areas of super- and subcritical reflection are also indicated in Fig. 6.

The amplitudes of incoming and reflected waves must satisfy the relation

$$\frac{a_r(\mathbf{k}^r)\mathbf{n}\cdot\mathbf{U}(\mathbf{k}^r)}{|v_3(\mathbf{k}^r)|} + \frac{a_i(\mathbf{k}^i)\mathbf{n}\cdot\mathbf{U}(\mathbf{k}^i)}{|v_3(\mathbf{k}^i)|} = 0 \tag{11.6}$$

where the representation of the internal wave field is analogous to (2.7). This relation becomes singular when $\mathbf{n}\cdot\mathbf{U} = 0$, which again occurs at the critical frequency ω_c. If a statistical ensemble is introduced, the

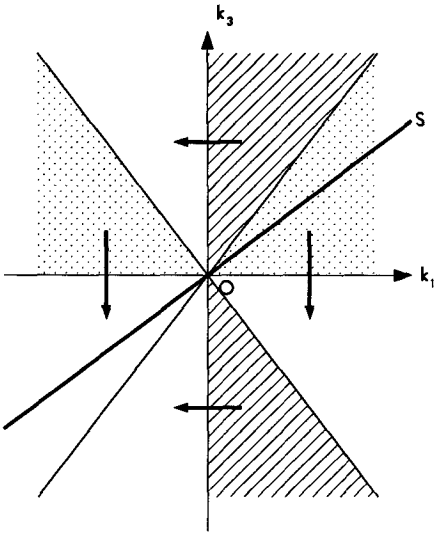

FIG. 6. Regions of permissible incident and reflective waves in the horizontal–vertical wavenumber plane. The heavy solid straight line represents the bottom slope. The light solid lines represent the critical frequency cone. The cross-hatched and stippled regions are permissible incident wavenumbers. For the cross-hatched regions the reflection is subcritical, for the stippled region the reflection is supercritical. The regions to which the incident wavenumbers become reflected are indicated by the arrows.

relation between reflected and incident energy density spectrum takes the simple form

$$\frac{E_r(k_1^r, k_3^r)}{E_i(k_1^i, k_3^i)} = \left(\frac{\mathbf{n}\cdot\mathbf{U}(\mathbf{k}^i)}{|v_3(\mathbf{k}^i)|}\right)^2\left(\frac{|v_3(\mathbf{k}^r)|}{\mathbf{n}\cdot\mathbf{U}(\mathbf{k}^r)}\right)^2 = 1 \quad (11.7)$$

which is equivalent to Eriksen's (1985) relation

$$\frac{E_r(\omega^r, k_3^r)}{E_i(\omega^i, k_3^i)} = \left(\frac{k_3^r}{k_3^i}\right)^2 \quad (11.8)$$

upon change of independent variables. These relations are of course equivalent to the condition

$$\frac{E_r(k_1^r, k_3^r)|\mathbf{n}\cdot\mathbf{v}(k_1^r, k_3^r)|\,dk_1^r dk_3^r}{E_i(k_1^i, k_3^i)|\mathbf{n}\cdot\mathbf{v}(k_1^i, k_3^i)|\,dk_1^i dk_3^i} = 1 \quad (11.9)$$

which states that there is no energy flux through the bottom. This statement has the same form in any representation.

For comparison with the scattering process we have to calculate the redistributed energy flux

$$D_r(\omega, \alpha) = F_r(\omega, \alpha) + F_i(\omega, \alpha) \quad (11.10)$$

as a function of frequency and horizontal wavenumber $\alpha = k_1$. Since for each value of ω and α there are two reflected waves with inclination θ_1 and $\theta_2[\theta = \arctan(k_3/k_1)]$ and two incident waves with inclinations θ_3 and θ_4, the redistributed energy flux is the sum of four terms

$$D_r(\theta, \alpha) = E_r(\theta_1, \alpha)v_n(\theta_1, \alpha) + E_r(\theta_2, \alpha)v_n(\theta_2, \alpha) - E_i(\theta_3, \alpha)v_n(\theta_3, \alpha) - E_i(\theta_4, \alpha)v_n(\theta_4, \alpha) \quad (11.11)$$

where

$$v_n(\theta, \alpha) = |\mathbf{n}\cdot\mathbf{v}| = \left|\frac{N^2 - f^2}{\omega\alpha}\sin\theta\cos^2\theta\cos(\theta - \varphi_0)\right| \quad (11.12)$$

is the magnitude of the normal component of the group velocity. In (θ, α) space the reflection laws take the form

$$\theta_r = \begin{cases} -\theta_i, & \text{for } \omega > \omega_c \\ -\theta_i - \pi, & \text{for } \omega < \omega_c \end{cases} \quad (11.13)$$

$$\frac{\alpha^r}{\alpha^i} = \left|\frac{\cos(\theta_r + \varphi_0)}{\cos(\theta_r - \varphi_0)}\right| \quad (11.14)$$

$$\frac{E_r(\theta_r, \alpha^r)}{E_i(\theta_i, \alpha^i)} = \frac{\alpha^r}{\alpha^i} \quad (11.15)$$

which imply

$$D_r(\omega, \alpha) = \sum_{i=1}^{2}\left(E_i\left(\omega, \alpha\left|\frac{\cos(\theta_i - \varphi_0)}{\cos(\theta_i + \varphi_0)}\right|\right) - E_i(\omega, \alpha)\right) \times v_n(\theta_i, \alpha)\cdot\left|\frac{\cos(\theta_i + \varphi_0)}{\cos(\theta_i - \varphi_0)}\right|. \quad (11.16)$$

Hence, the redistributed flux consists of two contributions. If we choose θ_1 to be in the third quadrant, then

$$\left|\frac{\cos(\theta_1 + \varphi_0)}{\cos(\theta_1 - \varphi_0)}\right| = R \leqslant 1, \quad (11.17)$$

and

$$\left|\frac{\cos(\theta_2 + \varphi_0)}{\cos(\theta_2 - \varphi_0)}\right| = R^{-1} \geqslant 1. \quad (11.18)$$

In the first contribution the reflected waves come from larger horizontal wavenumbers; in the second contribution from smaller horizontal wavenumbers. These two contributions are shown in Fig. 7 for a frequency $\omega = 1.5f$. The first contribution redistributes the energy flux from higher to lower wavenumbers, the second contribution from lower to higher wavenumbers. In total, there is a redistribution from medium toward lower and higher wavenumbers (Fig. 8). In Figs. 7 and 8 the bottom slope is $\gamma = 0.07$, implying a critical frequency $\omega_c = 1.2f$ for our standard parameters. When ω approaches the critical frequency, R becomes zero and waves are reflected to zero and infinite wavenumber.

The frequency-integrated redistributed energy flux $D_r(\alpha) = \int d\omega D_r(\alpha, \omega)$ is shown in Fig. 9. The flux is mainly redistributed from medium to higher wavenumbers with only a small fraction reflected to lower wavenumbers. The total flux in the positive (or negative) lobe is about 2.86 mW m^{-2}, about 15.7% of the incoming energy flux of 18.2 mW m^{-2}. Note that the

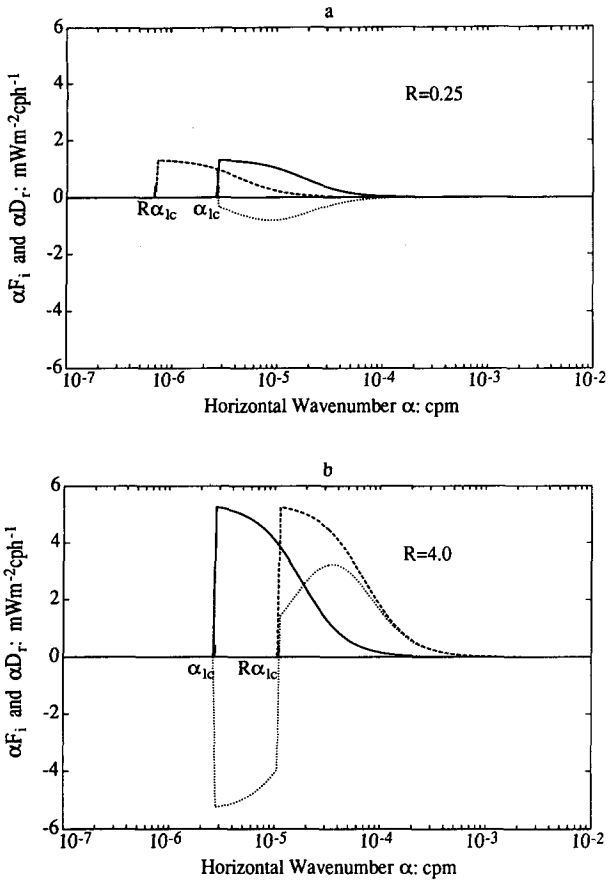

FIG. 7. The two contributions to the redistributed energy flux for the reflection process. The incident energy flux $|F_i(\alpha, \omega)|$ (solid line), the reflected energy flux $F_r(\alpha, \omega)$ (dashed line), and the redistributed flux $D_r(\alpha, \omega)$ (dotted line) are shown as a function of horizontal wavenumber α for frequency $\omega = 1.5f$ in a variance-conserving representation. The bottom slope is $\gamma = 0.07$ and the critical frequency is $\omega_c = 1.2f$. In case (a) the reflected waves have wavenumbers in the third quadrant. Reflection redistributes the energy flux from high to low wavenumbers. In case (b) the incident waves have wavenumbers in the first quadrant. Reflection redistributes the energy flux from low to high wavenumbers. The wavenumber α_{lc} is the low wavenumber cutoff of the internal wave spectrum.

incident energy fluxes differ slightly for the scattering and reflection process. For the scattering problem, the incident flux is the downward flux; for the reflection problem, the incident flux is the flux normal to the slope. Most of the redistribution comes from frequencies around the critical frequency. This is evident from Fig. 10, which shows the redistributed energy flux $D_r^+(\omega) = 1/2 \int d\alpha |D_r(\omega, \alpha)|$ as a function of frequency. The total redistributed energy flux is $D_r^+ = 3.89$ mW m^{-2}.

All our results are of course compatible with Eriksen's (1985) analysis of the reflection process. Here we have given the results in the (α_1, ω) representation in order to facilitate the comparison with the scattering process. The essence of this comparison is captured in Fig. 11, which compares $D(\alpha)$ for the reflection and scattering processes. Reflection redistributes a larger amount of the incoming energy flux than does scattering (2.86 mW m^{-2} as opposed to 1.07 mW m^{-2}).

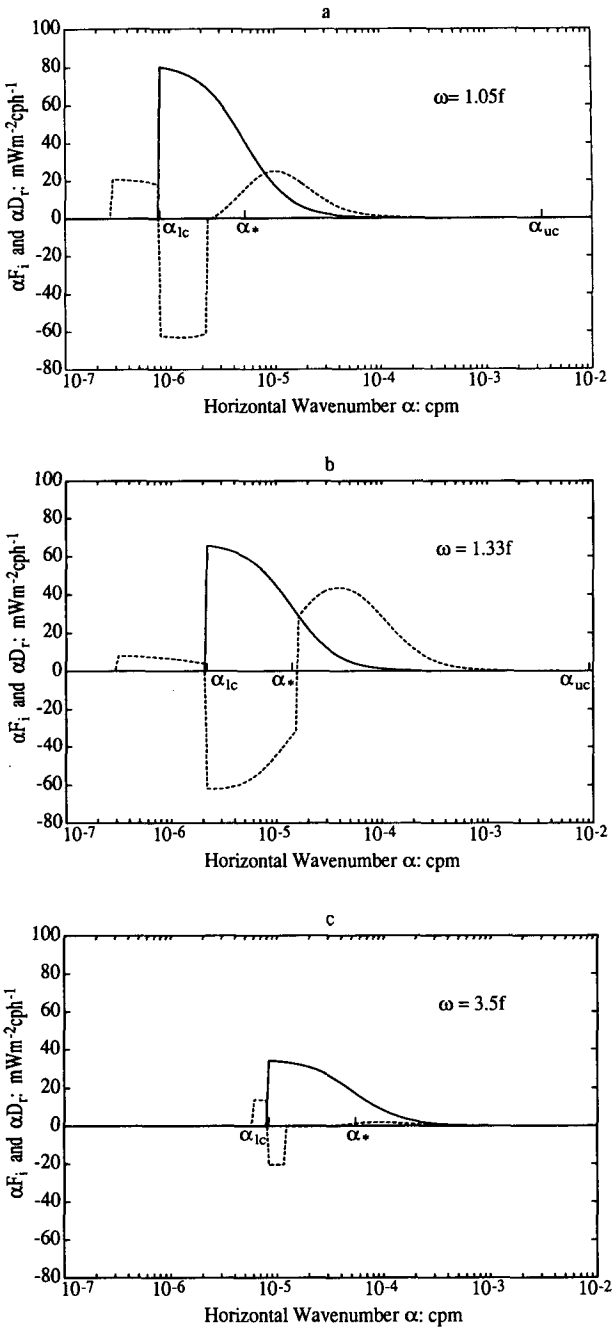

FIG. 8. Reflection at a straight slope. Incident energy flux $|F_i(\alpha, \omega)|$ (solid line) and redistributed energy flux $D_r(\alpha, \omega)$ (dashed line) as a function of horizontal wavenumber for three different frequencies in a variance-conserving representation. The bottom slope is $\gamma = 0.07$ and the critical frequency is $\omega_c = 1.2f$. The wavenumbers α_{lc}, α_*, and α_{uc} are the low wavenumber cutoff, bandwidth, and high wavenumber cutoff of the incident internal wave field, respectively.

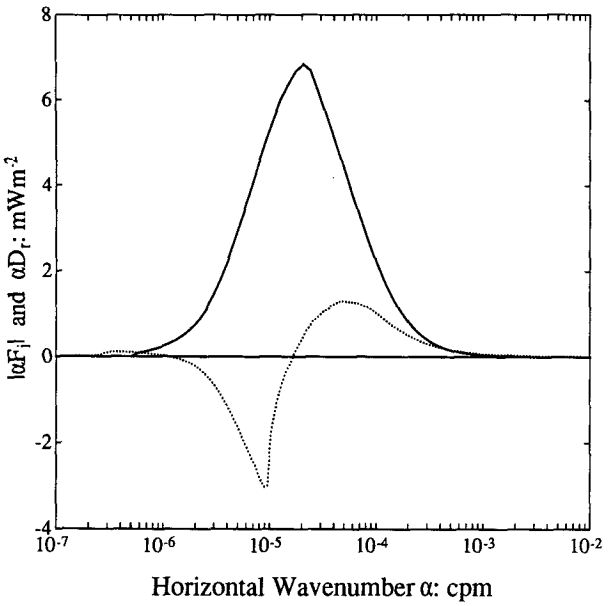

FIG. 9. Reflection at a straight slope. Incident energy flux $|F_i(\alpha)|$ (solid line) and redistributed energy flux $D_r(\alpha)$ (dotted line) as a function of horizontal wavenumber in a variance-conserving representation.

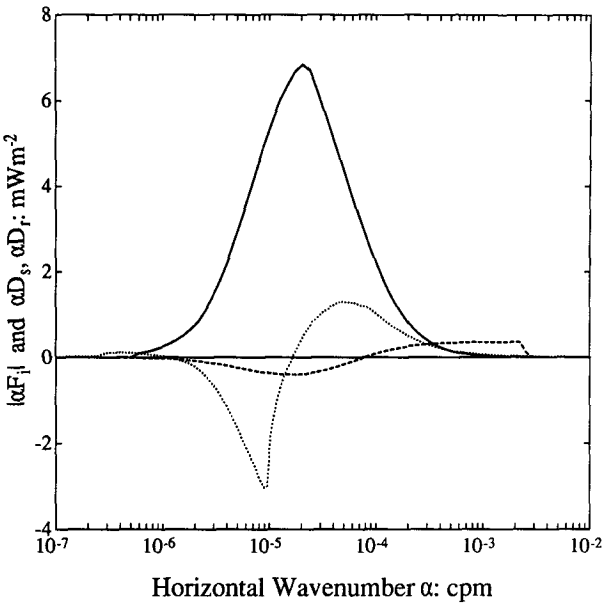

FIG. 11. Comparison of two-dimensional scattering and reflection. Incident energy flux $|F_i(\alpha)|$ (solid line), energy flux $D_s(\alpha)$ redistributed by scattering (dashed line), and energy flux $D_r(\alpha)$ redistributed by reflection (dotted line) in a variance-conserving representation.

However, scattering transfers the energy flux to much higher wavenumbers and might hence be more efficient than reflection in increasing the shear and inverse Richardson number. Indeed, Garrett and Gilbert (1988) find that the energy flux has to be transferred beyond a critical wavenumber $\alpha_c \approx 2 \times 10^{-4}$ cpm to lower the Richardson number below unity and to become available for mixing. Using this critical wavenumber we find that reflection liberates 0.25 mW m^{-2} for mixing, whereas scattering liberates 0.85 mW m^{-2}, more than three times as much! Of course, these numbers hold only for our standard parameters ($\gamma = 0.07$, $f = 0.042$ cph, $N = 0.4$ cph, etc.), which are supposed to represent typical ocean conditions. As shown in Garrett and Gilbert, the transfer to high wavenumbers by critical reflection is enhanced for steeper slopes and smaller f/N values. We find that scattering becomes more efficient for larger values of N and larger and more rugged topography.

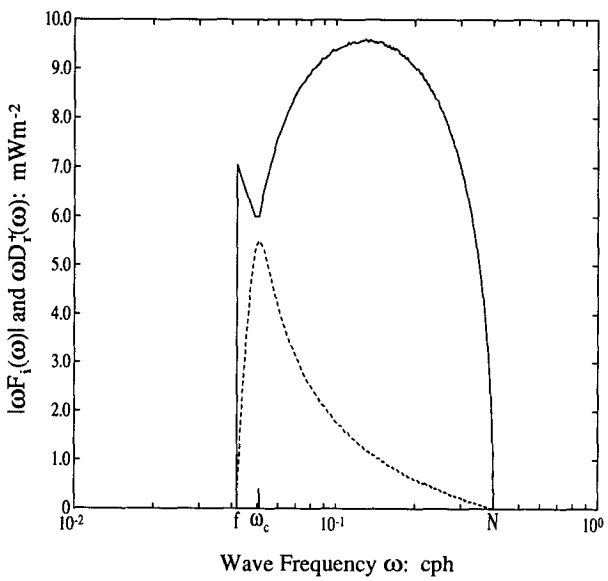

FIG. 10. Reflection at a straight slope. Incident energy flux $|F_i(\omega)|$ (solid line) and redistributed energy flux $D_r^+(\omega)$ (dashed line) as a function of frequency in a variance-conserving plot. The bottom slope is $\gamma = 0.07$ and the critical frequency is $\omega_c = 1.2f$.

12. Summary and conclusion

When internal waves interact with bottom topography, they change their horizontal wavenumber but not their frequency. There are at least two limiting cases where incoming low wavenumbers are changed to much larger outgoing wavenumbers. One process is reflection at a critical or near-critical slope. The other process is scattering at high-wavenumber bottom irregularities. In this paper we analyzed the scattering process and compared it to critical reflection analyzed previously by Eriksen (1982, 1985), Garrett and Gilbert (1988), and Gilbert and Garrett (1989). The scattering or reflection to high wavenumbers is of importance since high-wavenumber waves are likely to break and cause mixing. Such internal wave–induced mixing

near boundaries might significantly contribute to basinwide mixing and explain discrepancies between mixing observed in the ocean interior and required to satisfy basin heat and mass balances.

The scattering process was analyzed in the weak interaction limit where both waves and bottom Fourier components can be superimposed. The weak interaction limit requires the vertical wavelength to be larger than the bottom height and the wave slope to be larger than the bottom slope. For typical ocean conditions these conditions are only marginally satisfied, especially the slope condition, which breaks down for near-inertial waves. On the other hand, internal waves interacting with bottom topography tend to approach a statistical equilibrium, where for each frequency the energy flux is equipartitioned in horizontal wavenumber space. Indeed, we were able to explicitly prove an H theorem in the weak interaction limit. As the interaction between waves and topography becomes stronger, one expects the approach toward statistical equilibrium to be more efficient. Our weak interaction results might therefore represent lower bounds.

The derivation of the scattering integral in the weak interaction limit is straightforward but is given in this paper because previous results (Müller and Olbers 1975; Rubenstein 1988) contain algebraic errors. The efficiency of the scattering process is assessed by evaluating the scattering integral for a typical incident internal wave field [the Garrett and Munk 1976 spectral model (Desaubies 1976)] and for a typical bottom spectrum [Bell's (1975) spectral model]. The scattering process then redistributes about 6.8% of the incoming energy flux from low to high wavenumbers, mostly at near-inertial frequencies.

Comparison with the critical reflection process shows that the scattering process generally redistributes less energy flux but to higher wavenumbers. Scattering at high-wavenumber bottom irregularities might thus be equally or more efficient than critical reflection in causing boundary mixing.

Acknowledgments. This work relates to Department of Navy Grant N00014-89-J-1315 issued by the Office of Naval Research. The United States Government has a royalty-free license throughout the world in all copyrightable material contained herein.

REFERENCES

Baines, P. G., 1971a: The reflexion of internal/inertial waves from bumpy surfaces. *J. Fluid Mech.*, **46,** 273–291.

——, 1971b: The reflexion of internal/inertial waves from bumpy surfaces, part 2: Split reflexion and diffraction. *J. Fluid Mech.*, **49,** 113–131.

Bell, T. H., 1975: Statistical features of sea-floor topography. *Deep-Sea Res.*, **22,** 883–892.

Cairns, J. L., and G. O. Williams, 1976: Internal wave observations from a mid-water float, 2. *J. Geophys. Res.*, **81,** 1943–1950.

Cox, D., and H. Sandstrom, 1962: Coupling of internal and surface waves in water of variable depth. *J. Oceanogr. Soc. Japan* (20th Anniversary Volume), 499–513.

Desaubies, Y. J. F., 1976: Analytical representation of internal wave spectra. *J. Phys. Oceanogr.*, **6,** 976–981.

Eriksen, C. C., 1982: Observations of internal wave reflection off sloping bottoms. *J. Geophys. Res.*, **87,** 525–538.

——, 1985: Implications of ocean bottom reflection for internal wave spectra and mixing. *J. Phys. Oceanogr.*, **15,** 1145–1156.

Garrett, C. J. R., and D. Gilbert, 1988: Estimates of vertical mixing by internal waves reflected off a sloping bottom. *Small-Scale Turbulence and Mixing in the Ocean.* J. C. J. Nihoul and B. M. Jamart, Eds., 405–424.

Gilbert, D., and Garrett, C., 1989: Implications for ocean mixing of internal wave scattering off irregular topography. *J. Phys. Oceanogr.*, **19,** 1716–1729.

Müller, P., and D. J. Olbers, 1975: On the dynamics of internal waves in the deep ocean. *J. Geophys. Res.*, **80**(27), 3848–3860.

Munk, W. H., 1981: Internal waves and small-scale processes. *Evolution of Physical Oceanography,* B. A. Warren and C. Wunsch, Eds., MIT Press, 264–291.

Olbers, D. J., 1983: Models of the oceanic internal wave field. *Rev. Geophys. Space Phys.*, **20,** 1567–1606.

——, and N. Pomphrey, 1981: Disqualifying two candidates for the energy balance of oceanic internal waves. *J. Phys. Oceanogr.*, **11,** 1423–1425.

Rubenstein, D., 1988: Scattering of inertial waves by rough bathymetry. *J. Phys. Oceanogr.*, **18,** 5–18.